AMERICAN JOURNAL OF PHYSIOLOGY
GASTROINTESTINAL AND LIVER PHYSIOLOGY

Am J Physiol Gastrointest Liver Physiol 323: G165–G176, 2022.
First published June 21, 2022; doi:10.1152/ajpgi.00302.2021

RESEARCH ARTICLE

A novel maladaptive unfolded protein response as a mechanism for small bowel resection-induced liver injury

Allie E. Steinberger,[1]* Maria E. Tecos,[2]* Hannah M. Phelps,[1] Deborah C. Rubin,[3] Nicholas O. Davidson,[3] Jun Guo,[1] and Brad W. Warner[4]

[1]*Department of Surgery, Washington University School of Medicine, St. Louis, Missouri;* [2]*Department of Surgery, University of Nebraska Medical Center, Omaha, Nebraska;* [3]*Division of Gastroenterology, Department of Medicine, Washington University, St. Louis, Missouri; and* [4]*Division of Pediatric Surgery, Department of Surgery, Washington University School of Medicine, St. Louis Children's Hospital, St. Louis, Missouri*

Abstract

The unfolded protein response (UPR) is a complex adaptive signaling pathway activated by the accumulation of misfolded proteins in the endoplasmic reticulum (ER). ER stress (ERS) triggers a cascade of responses that converge upon C/EBP homologous protein (CHOP) to drive inflammation and apoptosis. Herein, we sought to determine whether liver injury and fibrosis after small bowel resection (SBR) were mediated by a maladaptive hepatic ERS/UPR. C57BL/6 mice underwent 50% proximal SBR or sham operation. Markers of liver injury and UPR/ERS pathways were analyzed. These were compared with experimental groups including dietary fat manipulation, tauroursodeoxycholic acid (TUDCA) treatment, distal SBR, and global CHOP knockout (KO). At 10 wk, proximal SBR had elevated alanine aminotransferase/aspartate aminotransferase (ALT/AST) ($P < 0.005$) and greater hepatic tumor necrosis factor-α (TNFα) ($P = 0.001$) and collagen type 1 α1 (COL1A1) ($P = 0.02$) than shams. SBR livers had increased CHOP and p-eIF2α, but were absent in activating transcription factor 4 (ATF4) protein expression. Low-fat diet (LFD), TUDCA, and distal SBR groups had decreased liver enzymes, inflammation, and fibrosis ($P < 0.05$). Importantly, they demonstrated reversal of hepatic UPR with diminished CHOP and robust ATF4 signal. CHOP KO-SBR had decreased ALT but not AST compared with wild-type (WT)-SBR ($P = 0.01$, $P = 0.12$). There were no differences in TNFα and COL1A1 ($P = 0.09$, $P = 0.50$). SBR-induced liver injury, fibrosis is associated with a novel hepatic UPR/ERS response characterized by increased CHOP and decreased ATF4. LFD, TUDCA, and ileocecal resection rescued the hepatic phenotype and reversed the UPR pattern. Global CHOP KO only partially attenuated liver injury. This underscores the significance of disruptions to the gut/liver axis after SBR and potentiates targets to mitigate the progression of intestinal failure-associated liver disease.

NEW & NOTEWORTHY The unfolded protein response (UPR) is a complex signaling cascade that converges upon C/EBP-homologous protein (CHOP). Under conditions of chronic cellular stress, the UPR shifts from homeostatic to proapoptotic leading to inflammation and cell death. Here, we provide evidence that small bowel resection-induced liver injury and fibrosis are mediated by a maladaptive hepatic UPR. Low-fat diet, TUDCA treatment, and ileocecal resection rescued the hepatic phenotype and reversed the UPR pattern.

ER stress; intestinal failure-associated liver disease; liver injury; short gut syndrome; unfolded protein response

INTRODUCTION

Short gut syndrome (SGS) is a disorder of nutrient malabsorption that follows a massive intestinal resection; a regrettably necessary treatment for many congenital disease processes such as necrotizing enterocolitis (NEC), congenital atresia, and midgut volvulus (1, 2). The severity of the disease is predicated on several factors, including remnant bowel length, presence of a competent ileocecal valve, intestinal continuity, and specific anatomic segmental involvement (3). Regardless, the associated morbidity is complex and significant, ranging from dehydration, metabolic derangements, and nutritional deficiencies to failure to thrive and death. Unfortunately, many children are unable to maintain adequate enteral nutrition and require intravenous alimentation. Despite marked structural and functional intestinal adaptation in the residual bowel, only 50% of children with SGS can wean to enteral autonomy (2).

Intestinal failure-associated liver disease (IFALD) is the most significant contributor to morbidity and mortality in infants and children with SGS. IFALD is a clinical spectrum characterized by cholestasis and steatosis with the potential to progress to fibrosis, cirrhosis, and liver failure. It is the leading indication for multivisceral organ transplantation (4). Once thought

*A. E. Steinberger and M. E. Tecos contributed equally to this work.
Correspondence: B. W. Warner (brad.warner@wustl.edu).
Submitted 7 October 2021 / Revised 10 May 2022 / Accepted 10 May 2022

to be primarily due to long-term parenteral nutrition, the drivers are likely multifactorial (5). Although lack of enteral stimulation, increased intestinal permeability, dysbiosis of the gut microbiome, disruption of the enterohepatic circulation, and systemic inflammation from sepsis play important roles, the exact pathogenesis is still largely unknown (5, 6).

The unfolded protein response (UPR) is a complex adaptive signaling pathway activated by the accumulation of misfolded proteins in the endoplasmic reticulum (ER). This ER stress (ERS) triggers three key UPR signal activator proteins, inositol requiring enzyme 1α/β (IRE1), PKR-like ER kinase (PERK), and activating transcription factor 6α/β (ATF6), which work in tandem to increase protein degradation and slow global protein translation in an effort to restore the cell to homeostatic conditions (7). However, when chronic or irreversible stress exceeds the capacity of this prosurvival mechanism, a cascade of responses converges on the C/EBP homologous protein (CHOP) transcription factor to drive cell death via apoptosis. This CHOP-mediated cell death leads to further impaired reduction-oxidation balance with resultant oxidative stress and significant inflammatory changes (8).

The biosynthetic function of the liver confers a particular susceptibility to ERS. Several studies in both human and animal models have demonstrated the critical role of maladaptive ERS and UPR in the development of acute and chronic liver diseases including IFALD (9). It has been postulated that the stimulation of lipogenesis in IFALD and the resultant production of reactive oxygen species could initiate the hepatocellular injury and inflammation which, if left unchecked, could lead to fibrosis (10).

We have previously reported marked liver injury and fibrosis in a TPN-independent murine model of proximal small bowel resection (SBR) (11, 12). As such, we sought to determine the role of the ERS response in this resection-associated liver damage. We hypothesized that hepatocellular injury with progression to fibrosis after proximal SBR is mediated by a maladaptive UPR response in the liver. We further posited that ameliorating the UPR through dietary or pharmacological intervention would mitigate liver injury after SBR.

METHODS

Mice

C57BL/6 (wild type, WT) and B6.129S(Cg)-*Ddit3*$^{tm2.1Dron}$/J (CHOP KO) 8-wk-old male mice were purchased from the Jackson Laboratory (Bar Harbor, ME) and housed in a temperature-controlled, pathogen-free animal holding facility on a 12-h light-dark cycle (St. Louis, MO). Mice were provided ample water and either SC (standard chow solid pellet, 13% kcal fat; PicoLab Rodent Diet 20, 53WU; LabDiet, St. Louis, MO) or liquid HFD (higher fat diet, 35% kcal fat; PMI Micro-Stabilized Rodent Liquid Diet LD 101; TestDiet, St. Louis, MO) ad libitum. Experiments were performed under protocol 20-0197 as approved by the Washington University Animal Studies Committee and followed the National Institutes of Health animal care guidelines.

Tauroursodeoxycholic Acid Administration

A cohort of mice (n = 7) was given tauroursodeoxycholic acid (TUDCA) (Calbiochem, La Jolla, CA) at a dose of 300 mg/kg/day in the liquid HFD and water daily for 10 wk. The control group was administered vehicle (i.e., water and HFD) without TUDCA. The mice were monitored daily, and no adverse effects were reported throughout the study period. The TUDCA dose of 300 mg/kg in mice corresponds to the human equivalent dose (HED) of 24.3 mg/kg as described in the literature (13, 14).

Tunicamycin Injection

A cohort of nonoperated mice (n = 4) was injected intraperitoneally with 1 mg/kg of tunicamycin (Sigma Aldrich, St. Louis, MO). These mice were harvested after 6 h, and liver samples were collected for analysis.

Operations

Mice underwent either a sham control operation, 50% proximal small bowel resection (SBR; jejunum), or 50% distal SBR (ileum). Preoperatively, mice were placed on the liquid HFD for 24 h. All surgeries were performed under isoflurane anesthesia. As previously described, sham operations involved transection of the bowel 12 cm proximal to the ileocecal junction with re-anastomosis alone (no bowel resection). A 50% proximal SBR was performed by transection of the small bowel 3–4 cm distal to the ligament of Treitz and ~12 cm proximal to the ileocecal junction (15). The intervening jejunum was removed. For distal resections, the bowel is transected 12 cm proximal to the ileocecal junction and just distal to the cecum, sparing the proximal colon (16). The intervening ileum and cecum were then removed. All anastomoses were constructed with a handsewn end-to-end anastomosis using interrupted 9-0 nylon sutures. Intraoperative (IO) samples of full-thickness small bowel were taken at the time of operation for histology. Mice from all groups were fed liquid HFD starting on a postoperative *day 1* for at least 1 wk as we have demonstrated that this is necessary to prevent anastomotic obstruction (15). Mice were then either transitioned to SC or maintained on HFD. Mice were euthanized at 2 and 10 wk postoperatively. Small bowel, colon, liver, and serum via submandibular venous puncture were collected at the time of harvest.

Adaptation

Intraoperative (IO) and postoperative (PO) intestinal tissue samples from corresponding segments of remnant small bowel were paraffin-embedded and stained with hematoxylin and eosin. To assess for structural adaptation, villus length and crypt depth were measured in at least 40 well-oriented crypts and villi at ×20 magnification by a single-blinded investigator (NIS elements AR 4; Nikon, Melville, NY), as previously described (17).

Hepatic Fibrosis Staining and Quantification

After formalin fixation and paraffin embedding, liver tissues were stained with Sirius red as a marker of fibrosis. The intensity of fibrotic staining was analyzed in a blinded manner by the same investigator.

F4/80 Immunohistochemistry Staining

Immunohistochemistry (IHC) was performed as described in Ref. 18. Briefly, the deparaffinized slides were blocked

with 3% hydrogen peroxide in methanol. Antigen retrieval was performed using Diva Decloaking solution (Biocare Medical, Concord, CA) (120°C for 2 min using a high-pressure cooker). Slides were blocked with avidin-pink and biotin-blue (Biocare Medical), treated with a specific antibody in DaVinci Green (Biocare Medical), incubated overnight at 4°C, and visualized with biotinylated goat anti-rabbit IgG (Jackson ImmunoResearch, Inc, West Grove, PA), followed by streptavidin-horseradish peroxidase (SA-5004-1; Vector Laboratories, Inc. Burlingame, CA), diaminobenzidine (SignalStain DAB Substrate Kit no. 8059; Cell Signaling Technology, Danvers, MA), and hematoxylin counterstaining. The antibody used in this study was F4/80 (No. 70076, 1:200; Cell Signaling Technology).

Real-Time PCR

Liver samples were isolated after harvest and homogenized in lysis buffer. RNA extraction was performed per the manufacturer's protocol (RNAqueous Kit, Ambion; Austin, TX). A NanoDrop Spectophotomer was used to measure sample RNA concentrations (ND-1000, NanoDrop Technologies; Wilmington, DE). *CHOP*, activating transcription factor 4 (*ATF4*), ATF6, spliced X-box-binding protein 1 (*XBP1s*), collagen type 1 α1 (*Col1A1*), tumor necrosis factor-α (*TNFα*) primers, and endogenous control primer *GAPDH* were purchased from Applied Biosystems (Life Technologies; Carlsbad, CA). RT-PCR was carried out via the Applied Biosystems 7500 Fast Real-Time PCR system. All results were normalized to the GAPDH endogenous control.

Western Blot

Total lysates were obtained by homogenization and protein concentration was determined with a protein assay RC DC kit (Bio-Rad; Hercules, CA). Samples were loaded into a 12% polyacrylamide gel, with Novex Sharp Pre-Stained Protein used as standard (Invitrogen; Carlsbad, CA). Dry transfer onto a nitrocellulose membrane (Invitrogen; Carlsbad, CA) was carried out via the iBLOT Gel Transfer Device (Invitrogen; Carlsbad, CA). Primary antibodies for CHOP, ATF4, ATF6, phosphorylated-eIF2α, XBP1s, cleaved caspase-3 and GAPDH, and rabbit secondary antibodies were purchased from Cell Signaling Technologies (Danvers, MA). The respective antibody dilutions used were ATF6 1:1,000; XBP1 1:2,500; CHOP 1:1,000; ATF4 1:1,000; GAPDH 1:10,000; p-eIF2a 1:1,000; and cleaved caspase-3 (9664 from CST) 1:50. The membrane was developed with Amersham ECL Western Blotting Detection Reagents (GE Healthcare; Chicago, IL). Protein detection and quantification were performed with Image Lab Software (Bio-Rad).

Statistical Analysis

Statistical analyses were performed using GraphPad-Prism 6 software (La Jolla, CA). Adaptation data were analyzed using an unpaired Student's *t* test. Serum alanine aminotransferase/aspartate aminotransferase (ALT/AST) and PCR relative gene expressions were analyzed using *t* tests or ANOVA with Fisher's LSD test for multiple comparisons. Normality was assessed and nonparametric tests were used where appropriate. Graphs show means and SD with significance. A P value of <0.05 was considered significant.

RESULTS

Given the association of chronic ERS with various liver diseases, we sought to determine the role of the UPR in our TPN-independent model of SBR-induced hepatic inflammation and fibrosis. We demonstrate that proximal SBR promotes a maladaptive ERS response leading to progressive liver injury at 10 wk. This UPR activation is limited to the PERK arm of the pathway, terminating in canonical executor protein, CHOP. Unique to this study, SBR leads to a paradoxical dissociation of CHOP from its upstream effector ATF4, resulting in an inverse relationship. A low-fat diet, conjugated bile acid supplementation, and selective distal resection, all ameliorated the ERS response and reversed CHOP/ATF protein expression, thereby mitigating the hepatic injury phenotype. Despite this, global suppression of CHOP via genetic knockout was not independently sufficient for suppressing hepatocellular injury and fibrosis after proximal SBR.

SBR Activates PERK Arm of UPR in Liver and Is Associated with Hepatic Injury Progressing to Fibrosis

After 10 postoperative weeks, villus height and crypt depth significantly increased in the remnant bowel of all resected mice, confirming structural intestinal adaptation ($P < 0.001$ and $P < 0.0001$, respectively; Fig. 1*A*). We confirmed the incidence and extent of liver injury and fibrosis after proximal SBR on HFD when compared with sham controls (11, 12). To evaluate for biochemical evidence of liver injury, serum ALT and AST were quantified. The SBR group demonstrated the elevation in ALT and AST compared with shams (48.8 ± 10.9 vs. 158.4 ± 19.3, $P = 0.001$ and 136.0 ± 44.5 vs. 389.1 ± 64.8, $P = 0.0129$, respectively; Fig. 1*B*). The SBR group was also found to have a greater inflammatory milieu by increased mRNA expression of *TNFα* in the liver ($P = 0.001$; Fig. 1*C*) as well as a higher percentage of hepatic F4/80-stained cells by immunohistochemistry ($P < 0.005$; Fig. 1*E*). Notably, resected mice showed significant liver fibrosis by Sirius Red staining histologically (Fig. 1*E*), which correlated with increased hepatic *Col1a1* mRNA expression ($P = 0.02$; Fig. 1*C*).

Next, we sought to characterize the UPR profile in the liver from both the SBR and sham-control groups at 10 wk. As shown in Fig. 1*D*, resected mice were noted to have significantly increased *CHOP* mRNA expression compared with shams (1.1 ± 0.1 vs. 3.2 ± 0.4, $P = 0.007$), suggesting induction of ER stress and activation of the UPR. Interestingly, there was no difference in hepatic ATF4, ATF6, or *XBP1s* mRNA expression between the groups (Fig. 1*D*). At the protein level, there was robust redemonstration of hepatic expression of CHOP and phosphorylated-eIF2α (p-eIF2α); however, ATF4 signal was nearly absent in the resected mice (Fig. 1*F*). This pattern of UPR activation was not seen in the sham controls, which exhibited increased ATF4 relative to SBR, but diminished CHOP and p-eIF2α. There was also evidence of increased apoptosis in SBR livers, revealed by highly expressed cleaved caspase-3 protein expression (Fig. 1*F*). This finding is consistent with prolonged ER stress and the resultant initiation of the CHOP-associated apoptotic pathways. The expression of other canonical UPR pathways, such as ATF6 and XBP1 were not elevated after SBR or sham at the protein level (data not shown). Importantly, all arms of the

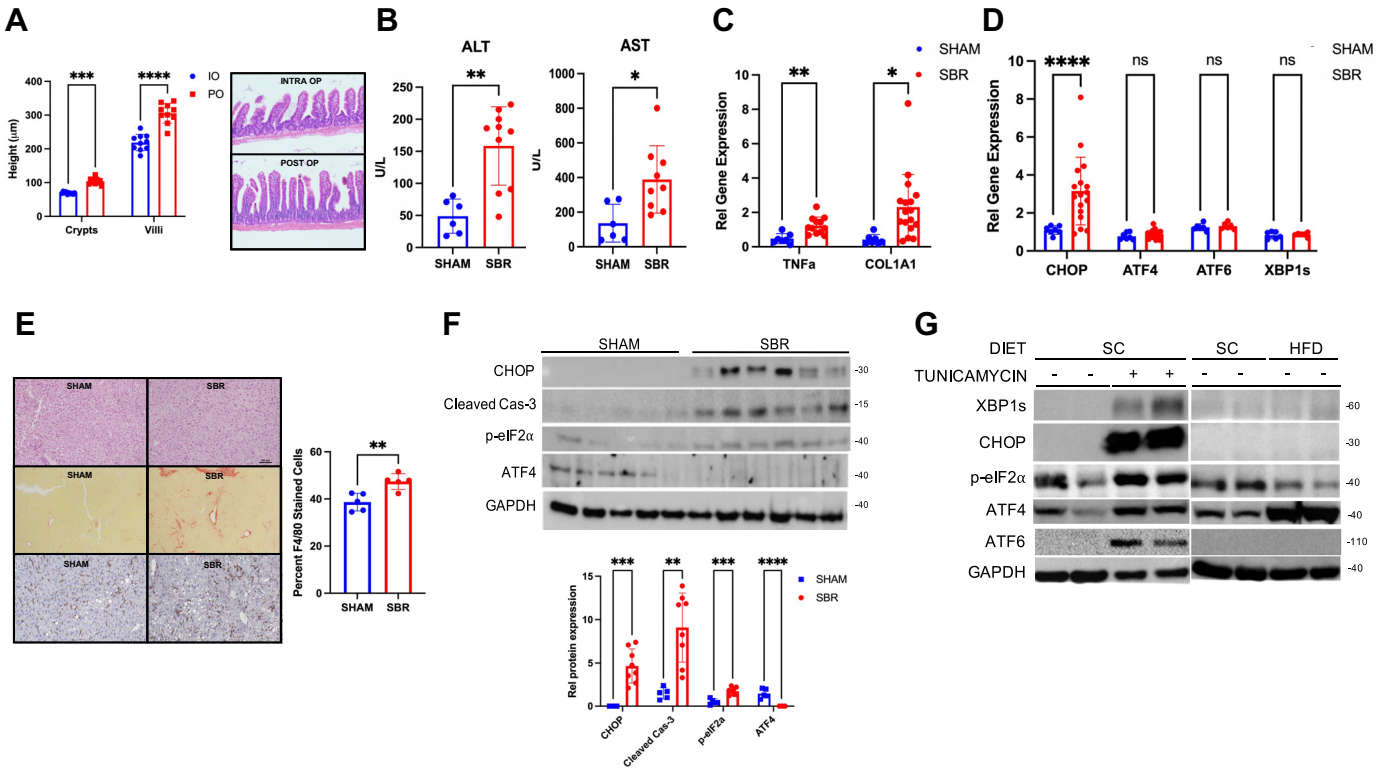

Figure 1. SBR activates PERK arm of UPR in liver and is associated with hepatic injury that progresses to fibrosis at 10 wk on HFD. *A*: confirmation of structural adaptation with representative histological intraoperative (IO) and postoperative (PO) images at ×10 magnification. *B*: serum ALT and AST in sham vs. SBR on HFD. *C*: RT-PCR for TNFα, COL1A1 in sham vs. SBR. *D*: RT-PCR relative expression levels for CHOP, ATF4, ATF6, XBP1s in sham vs. SBR livers on HFD. *E*: representative images of H&E, Sirius Red, and F4/80 IHC staining in liver at ×20 magnification. *F*: Western blot results for CHOP, cleaved caspase-3, p-eIF2α, ATF4, and GAPDH in sham vs. SBR on HFD with quantification of relative protein expression. *G*: Western blot results for XBP1s, CHOP, p-eIF2α, ATF4, ATF6, and GAPDH in nonoperated tunicamycin-injected and nonoperated, noninjected SC vs. HFD-fed mice. All data are shown as means ± SD. $*P < 0.05$, $**P < 0.005$, $***P < 0.0005$, and $****P < 0.0001$. ALT, alanine aminotransferase; AST, aspartate aminotransferase; ATF, activating transcription factor; COL1A1, collagen type 1 α1; CHOP, C/EBP homologous protein; GAPDH, glyceraldehyde-3-phosphate dehydrogenase; HFD, higher fat diet; H&E, hematoxylin and eosin; IHC, immunohistochemistry; PERK, PKR-like ER kinase; RT-PCR, reverse transcription-polymerase chain reaction; SBR, small bowel resection; TNFα, tumor necrosis factor-α; UPR, unfolded protein response; XBP1s, X-box-binding protein 1.

UPR were observed in livers of nonoperated mice harvested after 6 h of stimulation with tunicamycin, a known ER stress-inducing drug (Fig. 1*G*), confirming that these adaptive pathways are detectable. In addition, neither SC nor HFD alone in nonoperated mice induced the UPR based on relative CHOP expression in the liver (Fig. 1*G*).

Diet-Mitigated Liver Fibrosis in SBR Is Associated with Diminished CHOP Expression

We showed that the phenotype of progressive liver injury with fibrosis following SBR can be attenuated by a low-fat diet (12). To further investigate the effects of dietary manipulation and resection-associated liver injury on the UPR, a cohort of proximal SBR mice (n = 10) was transitioned to a low-fat SC diet at postoperative *day 7* and the outcomes were compared with SBR and sham-operated groups on liquid HFD. Structural adaptation was confirmed in the remnant bowel of all resected mice ($P < 0.05$; Fig. 2*A*). At 2 wk, the SBR cohort on HFD had significantly elevated serum ALT and AST (sham HFD 52.6 + 4.9 vs. SBR HFD 343.7 ± 59.7, P = 0.0003; sham HFD 118.9 + 16.7 vs. SBR HFD 556.8 ± 60.3, $P < 0.0001$; Fig. 2*B*), with inflammation as inferred by increased mRNA expression of hepatic *TNFα* (P = 0.0006; Fig. 2*C*) when compared with sham counterparts on HFD. Notably, this HFD-induced liver injury after SBR was mitigated when mice were fed SC for 1 wk as evidenced by decreased serum enzymes (ALT: SBR HFD 343.7 ± 59.7 vs. SBR SC 105.1 ± 36.2, P = 0.0003; AST: SBR HFD 556.8 ± 60.3 vs. SBR SC 244.9 ± 39.5, $P < 0.0001$; Fig. 2*B*), decreased hepatic *TNFα* mRNA expression (P = 0.0006; Fig. 2*C*), and decreased Sirius Red staining on liver histology (Fig. 2*D*).

Liver injury in the HFD-SBR group was associated with increased hepatic *CHOP* mRNA expression (P = 0.0199; Fig. 2*E*) compared with both shams and SBR on SC. Furthermore, there was no difference in *ATF4* mRNA between sham and SBR on HFD (P = 0.7317), but there was significantly decreased *ATF4* expression in the livers of the SC-SBR group (HFD-SBR vs. SC-SBR, P = 0.0017 and HFD-sham vs. SC-SBR, P = 0.0034; Fig. 2*E*). On Western blot, the SBR cohort on HFD (with hepatic inflammation and damage) exhibited increased CHOP and p-eIF2α expression, but no detectable ATF4 protein (Fig. 2*F*). This pattern was like that of the resected mice at 10 wk (Fig. 1*E*). Interestingly, the SC-SBR group (where a low-fat diet abrogated the liver injury phenotype) exhibited reduced CHOP and p-eIF2α protein expression, whereas ATF4 protein expression was readily detectable, despite the relative reduction in transcript abundance (Fig. 2, *E* and *F*). These findings suggest that posttranscriptional

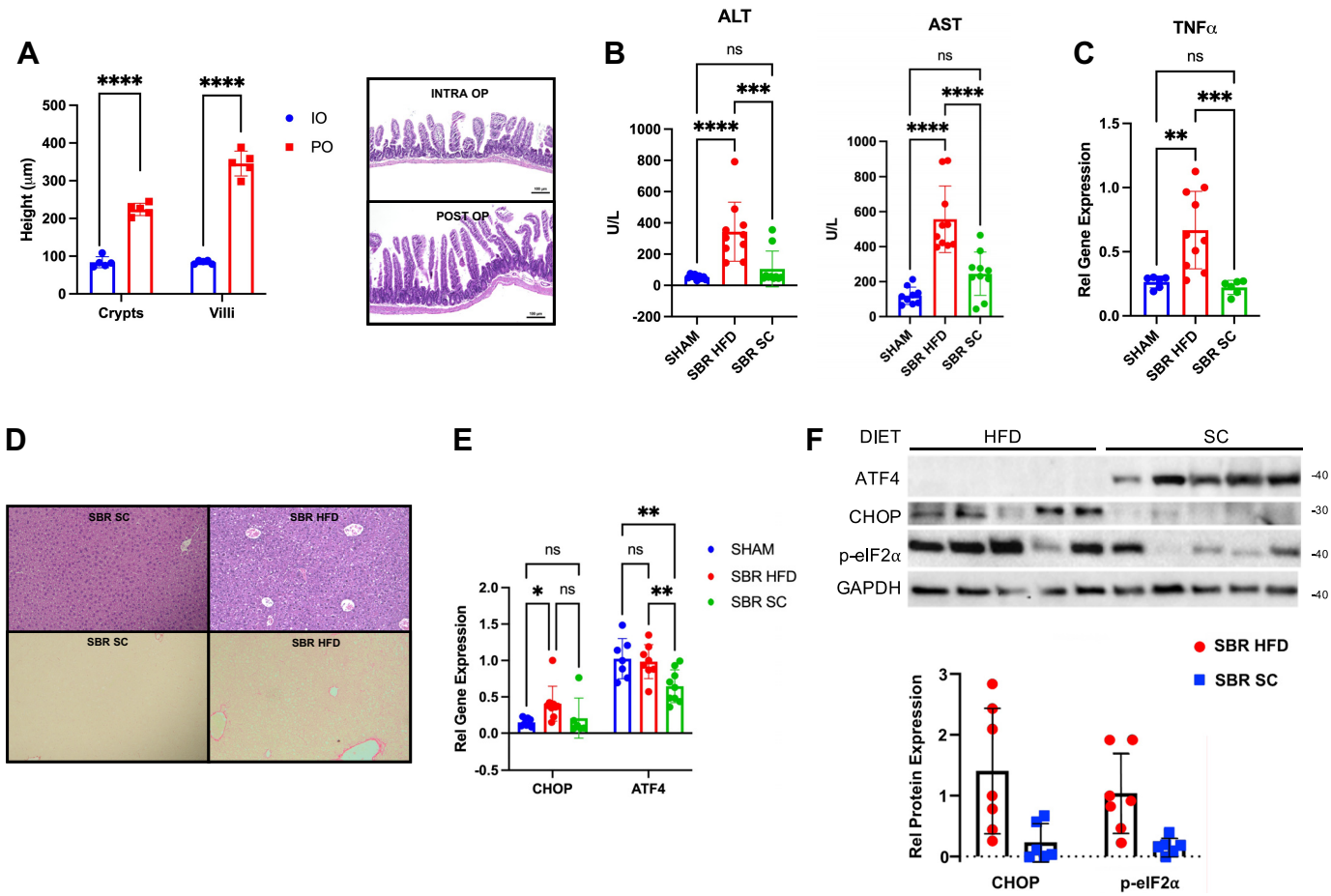

Figure 2. Diet-mitigated liver fibrosis in SBR is associated with diminished CHOP expression at 2 wk. *A*: confirmation of structural adaptation with representative histological intraoperative (IO) and postoperative (PO) images at ×10 magnification. *B*: serum ALT and AST in sham vs. SBR-HFD vs. SBR-SC. *C*: RT-PCR for relative expression levels of TNFα in sham vs. SBR-HFD vs. SBR-SC livers. *D*: representative images of H&E and Sirius Red staining in liver at ×20 magnification. *E*: RT-PCR for relative expression levels of CHOP, ATF4 in sham vs. SBR-HFD vs. SBR-SC livers. *F*: Western blot results for ATF4, CHOP, p-eIF2α, and GAPDH in SBR-HFD vs. SBR-SC at 2 wk with quantification of relative protein expression. All data are shown as means ± SD. $*P < 0.05$, $**P < 0.005$, $***P < 0.0005$, and $****P < 0.0001$. ALT, alanine aminotransferase; AST, aspartate aminotransferase; ATF, activating transcription factor; COL1A1, collagen type 1 α1; CHOP, C/EBP homologous protein; GAPDH, glyceraldehyde-3-phosphate dehydrogenase; HFD, higher fat diet; H&E, hematoxylin and eosin; IHC, immunohistochemistry; PERK, PKR-like ER kinase; RT-PCR, reverse transcription-polymerase chain reaction; SC, standard chow; SBR, small bowel resection; TNFα, tumor necrosis factor-α.

regulatory steps in ATF4 expression may play an important role in regulating elements of the UPR and ERS response.

TUDCA Is Hepatoprotective after SBR and Reverses the CHOP/ATF4 Expression Profile

TUDCA has been shown to decrease ER stress and correct subsequent dysregulation of the UPR, thereby mitigating the detrimental effects of a chronic proapoptotic and proinflammatory milieu in the liver (13, 19, 20). To evaluate the potential therapeutic effects on resection-associated liver injury, TUDCA was administered (300 mg/kg/day in liquid HFD and water) to a cohort of 50% proximal SBR mice ($n = 7$) daily for 10 wk.

Postoperative structural adaptation was confirmed in all samples (crypts: $P < 0.0001$ and villi: $P < 0.0001$; Fig. 3*A*). At 10 wk, TUDCA-treated SBR mice demonstrated reduced liver injury compared with vehicle HFD-SBR and sham-operated controls. This was evidenced by reduced serum ALT and AST (sham 48.83 vs. SBR 158.4 vs. TUDCA-SBR 58.00 ± 24.51, $P = 0.0002$ and sham 136.0 vs. SBR 475.0 vs. TUDCA-SBR 175.7 ± 122.4, $P = 0.0049$; Fig. 3*B*), abrogation of inflammation by decreased hepatic *TNFα* mRNA expression ($P = 0.0004$; Fig. 3*C*), and a nonsignificant decrease in the percentage of hepatic F4/80-stained cells on IHC ($P = 0.07$; Fig. 3*D*). Furthermore, TUDCA-SBR mice showed significant attenuation of liver fibrosis with decreased *Col1a1* mRNA expression ($P = 0.0004$; Fig. 3*C*) and minimal parenchymal collagen deposition of Sirius Red staining by histology (Fig. 3*D*).

Given that TUDCA rescued the SBR-associated liver phenotype and is known to attenuate ER stress, we next interrogated the hepatic UPR activation in this cohort. TUDCA-treated SBR mice exhibited lower relative mRNA expression of hepatic *CHOP* compared with vehicle control-SBR mice ($P = 0.0006$; Fig. 3*E*), consistent with mitigated ER stress. However, there was no difference in *ATF4* mRNA abundance (Fig. 3*E*). Hepatic protein expression in the TUDCA-SBR cohort revealed a complete reversal of the UPR pattern expressed by the untreated SBR cohort, with a nearly undetectable CHOP signal yet readily detectable expression of

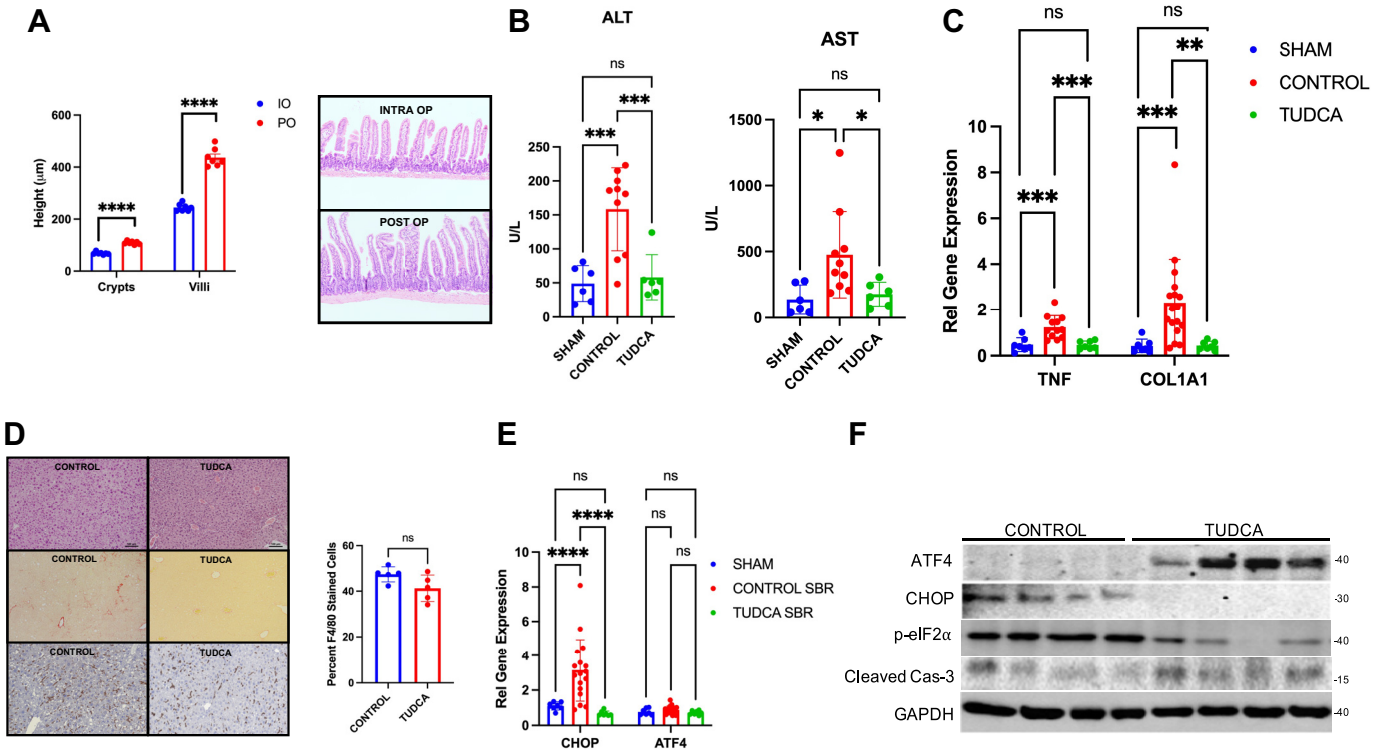

Figure 3. TUDCA is hepatoprotective after SBR and reverses pattern of CHOP/ATF4 expression at 10 wk. *A*: confirmation of structural adaptation with representative histological intraoperative (IO) and postoperative (PO) images at ×10 magnification. *B*: serum ALT and AST in sham vs. vehicle control-SBR vs. TUDCA-SBR. *C*: RT-PCR for TNFα, COL1A1 in sham vs. vehicle control-SBR vs. TUDCA-SBR. *D*: representative images of H&E, Sirius Red, and F4/80 IHC staining in vehicle control-SBR and TUDCA-SBR livers at ×20 magnification. *E*: RT-PCR relative expression levels for CHOP, ATF4 in sham vs. vehicle control-SBR vs. TUDCA-SBR livers. *F*: Western blot results for ATF4, CHOP, p-eIF2α, cleaved caspase-3, and GAPDH in sham vs. vehicle control-SBR vs. TUDCA-SBR livers. All data are shown as means ± SD. $*P < 0.05$, $**P < 0.005$, $***P < 0.0005$, and $****P < 0.0001$. Vehicle control was HFD alone and treatment-group was HFD and TUDCA. ALT, alanine aminotransferase; AST, aspartate aminotransferase; ATF, activating transcription factor; COL1A1, collagen type 1 α1; CHOP, C/EBP homologous protein; GAPDH, glyceraldehyde-3-phosphate dehydrogenase; HFD, higher fat diet; H&E, hematoxylin and eosin; IHC, immunohistochemistry; RT-PCR, reverse transcription-polymerase chain reaction; SBR, small bowel resection; TNFα, tumor necrosis factor-α; TUDCA, tauroursodeoxycholic acid.

ATF4 (Fig. 3*F*). Despite this, there was no difference in apoptotic rate by cleaved caspase-3 protein expression (Fig. 3*F*). This UPR pattern is consistent with our abovementioned hepatoprotective findings in our diet-manipulated cohort (Fig. 2, *E* and *F*), which mimic sham-operated control UPR intermediary expression patterns. The findings again point to the importance of posttranscriptional regulation of ATF4 expression.

Distal SBR Mitigates Hepatic Injury and Halts Progression to Fibrosis via UPR Manipulation

We have previously reported enhanced adaptation in both the remnant small bowel and colonic tissues of our distal SBR when compared with our proximal SBR model (16). As such, we sought to investigate whether these changes contributed to further modulation of the UPR axis, and if varying locus-based resection models result in different hepatic phenotypes.

Profiles of resection-associated liver injury between proximal and distal SBR were then directly compared. Structural adaptation was again confirmed histologically (crypts: $P = 0.0002$ and villi: $P < 0.0001$; Fig. 4*A*). Serum ALT and AST were significantly decreased in the distal SBR cohort when compared with their proximal SBR counterparts ($P = 0.0005$ and $P = 0.0077$, respectively; Fig. 4*B*), serologically mirroring the serum levels of sham-operated mice. Overall hepatic inflammation was assessed and was found to be markedly reduced in distal SBR versus proximal SBR livers by mRNA expression of *TNFα* ($P < 0.0001$; Fig. 4*C*) and F4/80 staining ($P < 0.0001$; Fig. 4*D*). This directly correlated with decreased hepatic fibrosis as evidenced by both hepatic expression of *Col1a1* ($P < 0.0001$; Fig. 4*C*) and Sirius Red staining (Fig. 4*D*). Taken together, this provides evidence that distal SBR alone abrogates the liver injury phenotypes associated with ER stress and subsequent UPR activation initiated by proximal SBR. This hepatoprotective state after distal SBR is comparable to the profile demonstrated in sham-operated controls.

Attention was then turned to the pattern of UPR activation in the liver. Interestingly, despite the observed phenotypic differences in hepatic injury, there was equivalent expression of *CHOP* in both proximal and distal SBR livers at the RNA level ($P = 0.8853$; Fig. 4*E*). Furthermore, hepatic *CHOP* was elevated in distal SBR when compared with sham-operated mice ($P = 0.0046$; Fig. 4*E*). Hepatic *ATF4* expression was not significantly different among the cohorts (proximal vs. distal SBR, $P = 0.4661$ and distal SBR vs. sham, $P = 0.1898$; Fig. 4*E*). To further characterize hepatic UPR expression and specifically investigate the activation of the PERK arm,

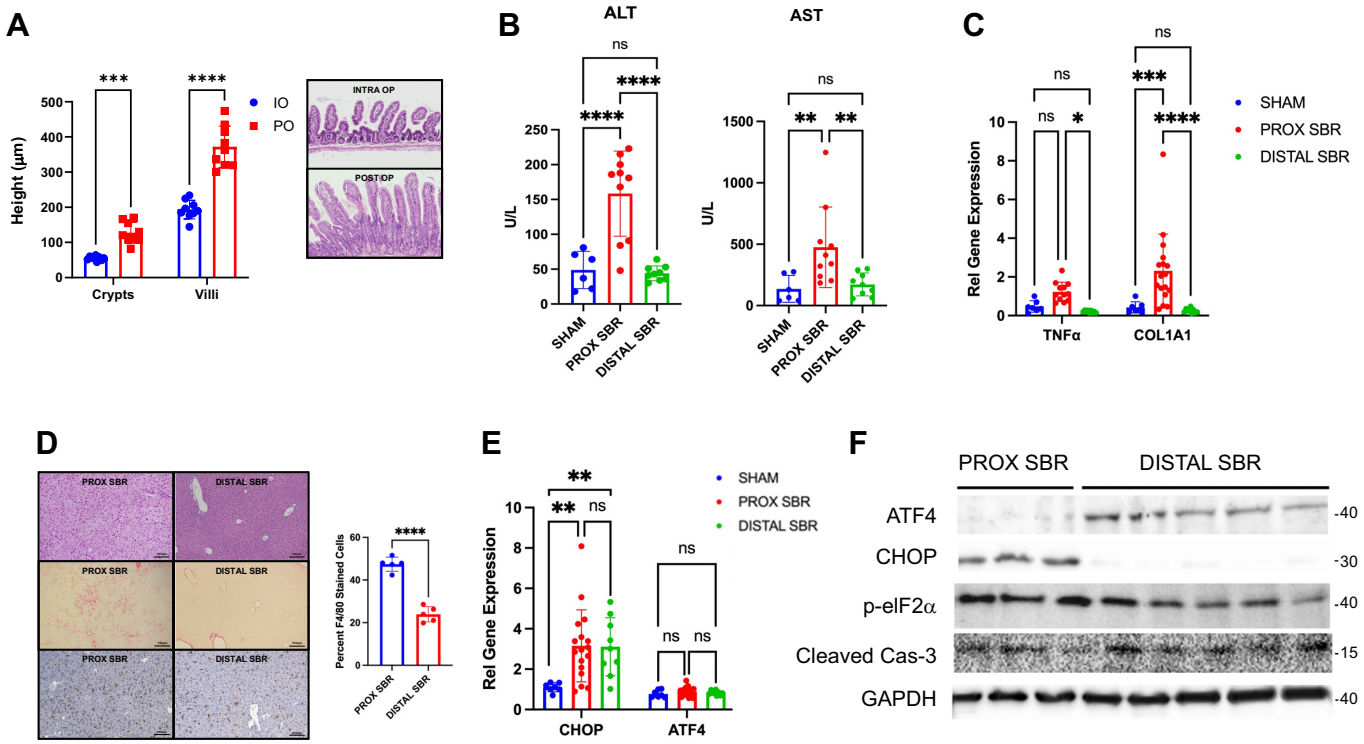

Figure 4. Distal resection mitigates hepatic injury and halts progression to fibrosis via UPR manipulation at 10 wk. *A*: confirmation of structural adaptation with representative histological intraoperative (IO) and postoperative (PO) images at ×10 magnification. *B*: serum ALT and AST in sham vs. proximal SBR vs. distal SBR on HFD. *C*: RT-PCR relative gene expression for TNFα, COL1A1 in sham vs. proximal SBR vs. distal SBR on HFD. *D*: representative images of H&E, Sirius Red, and F4/80 IHC staining in proximal SBR vs. distal SBR livers at ×20 magnification. *E*: RT-PCR relative expression levels for CHOP, ATF4 in sham vs. proximal SBR vs. distal SBR livers on HFD. *F*: Western blot results for ATF4, CHOP, p-eIF2α, cleaved caspase-3, and GAPDH in sham vs. proximal SBR vs. distal SBR livers on HFD. All data are shown as means ± SD. $*P < 0.05$, $**P < 0.005$, $***P < 0.0005$, and $****P < 0.0001$. ALT, alanine aminotransferase; AST, aspartate aminotransferase; ATF, activating transcription factor; COL1A1, collagen type 1 α1; CHOP, C/EBP homologous protein; GAPDH, glyceraldehyde-3-phosphate dehydrogenase; HFD, higher fat diet; H&E, hematoxylin and eosin; IHC, immunohistochemistry; PERK, PKR-like ER kinase; RT-PCR, reverse transcription-polymerase chain reaction; SBR, small bowel resection; TNFα, tumor necrosis factor-α; UPR, unfolded protein response.

protein expression was evaluated. In the distal SBR group, a negligible CHOP signal was identified despite robust ATF4 activation (Fig. 4*F*). There was no difference in cleaved-caspase 3 protein expression (Fig. 4*F*). These end-protein product level findings are a critical redemonstration of UPR pathway arrest resulting in hepatoprotection. Discordance of mRNA and protein expression of PERK pathway intermediaries may indicate a higher level regulation of UPR functioning necessary to induce SBR-associated hepatic injury. These findings again highlight the consequence of posttranscriptional regulation of ATF4 expression.

CHOP KO Partially Mitigates Hepatic Phenotype after SBR

Because of the strong correlation between CHOP expression and liver injury, we sought to determine whether CHOP (the canonical executor protein of the maladaptive UPR) was required for the SBR-associated hepatic phenotype. A cohort of global CHOP KO mice underwent 50% proximal SBR ($n = 7$) and was compared with wild-type (WT) sham and WT-SBR controls at 10 wk. All mice were fed liquid HFD for the duration of the postoperative course. As before, structural adaptation was confirmed in the CHOP KO-SBR by comparing IO with PO intestinal histology (crypts: $P < 0.0001$; villi: $P < 0.0001$; Fig. 5*A*). Biochemically, CHOP KO-SBR had decreased serum ALT levels compared with WT-SBR controls (158.4 vs. 92.33 ± 66.07, $P = 0.012$; Fig. 5*B*) but no difference in AST ($P = 0.1209$; Fig. 5*B*). Though lower, there was no statistical difference in the relative mRNA expression levels of *TNFα* (sham 0.47 ± 0.29. WT-SBR 1.23 ± 0.50 vs. CHOP KO-SBR 0.76 ± 0.58, $P = 0.094$; Fig. 5*C*) or hepatic F4/80 staining ($P = 0.22$; Fig. 5*D*) between CHOP KO and WT-SBR groups. Finally, although there was a nonsignificant decrease in *Col1A1* mRNA expression in CHOP KO livers compared with WT-SBR (2.31 vs. 1.83, $P = 0.50$; Fig. 5*C*), diminished fibrotic staining with Sirius Red was observed (Fig. 5*D*). These observations are concordant with reported attenuation, but not complete prevention, of UPR signaling in other CHOP KO models (21).

CHOP KO was then confirmed by PCR ($P < 0.001$; Fig. 5*E*). Of note, hepatic *ATF4* mRNA expression was markedly elevated in CHOP KO-SBR relative to the WT-SBR and WT-sham cohorts ($P = 0.003$, $P = 0.001$; Fig. 5*E*). CHOP KO was recapitulated by lack of CHOP protein expression on Western blot. Compared with WT-SBR, the CHOP KO-SBR group highly expressed ATF4 protein in the liver, commensurate to our abovementioned RNA findings (Fig. 5*F*). Of note, this is the first experimental condition in which hepatic ATF4 RNA and protein expression are directionally aligned. In all previous cohorts, there has been a disconnect between relative ATF4 mRNA and protein levels with translational products closely correlating to the degree of liver injury. (Fig. 5, *E* and *F*). There was a difference in apoptotic rate by

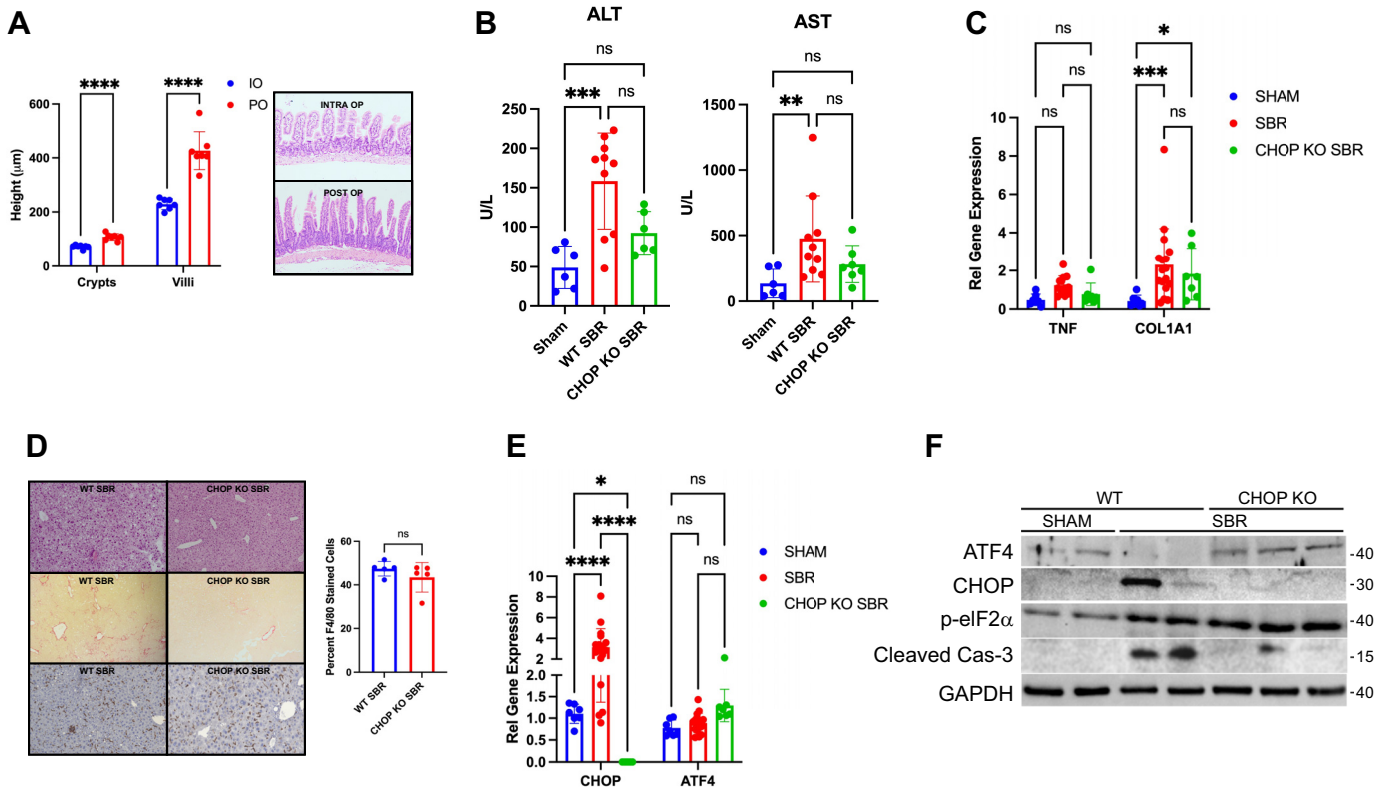

Figure 5. CHOP KO partially mitigates hepatic phenotype after resection but is not essential at 10 wk. *A*: confirmation of structural adaptation with representative histological images of CHOP KO intraoperative (IO) and CHOP KO postoperative (PO) at ×10 magnification. *B*: serum ALT and AST in WT-sham vs. WT-SBR vs. CHOP KO-SBR on HFD. *C*: RT-PCR for TNFα, COL1A1 in WT-sham vs. WT-SBR vs. CHOP KO-SBR on HFD. *D*: representative images of H&E, Sirius Red, F4/80 IHC staining in WT-SBR, and CHOP KO-SBR livers at ×20 magnification. *E*: RT-PCR relative expression levels for CHOP, ATF4 in WT-sham vs. WT-SBR vs. CHOP KO-SBR livers on HFD. *F*: Western blot results for ATF4, CHOP, p-eIF2α, cleaved caspase-3, and GAPDH WT-sham vs. WT-SBR vs. CHOP KO-SBR livers on HFD. All data are shown as means ± SD. $*P < 0.05$, $**P < 0.005$, $***P < 0.0005$, and $****P < 0.0001$. ALT, alanine aminotransferase; AST, aspartate aminotransferase; ATF, activating transcription factor; COL1A1, collagen type 1 α1; CHOP, C/EBP homologous protein; GAPDH, glyceraldehyde-3-phosphate dehydrogenase; HFD, higher fat diet; H&E, hematoxylin and eosin; KO, knockout; IHC, immunohistochemistry; PERK, PKR-like ER kinase; RT-PCR, reverse transcription-polymerase chain reaction; SBR, small bowel resection; TNFα, tumor necrosis factor-α; WT, wild type.

cleaved caspase-3 expression. CHOP KO-SBR had protein levels similar to sham WT controls, both markedly decreased when compared with WT-SBR (Fig. 5*F*).

DISCUSSION

In this study, the resultant proximal resection milieu triggered ER stress and led to the selective induction of the PERK arm of the UPR. Activation of this maladaptive UPR was associated with increased hepatic expression of canonical executor protein CHOP and reciprocal reduction of ATF4. This represents a unique PERK-specific terminal response that is dissociated from upstream ATF4 activity. Protracted ERS resulted in a commensurate resection-associated liver injury and fibrosis that was not seen in sham controls. The hepatic damage was mitigated by a low-fat diet, TUDCA treatment, and distal SBR with a reversal in the CHOP-ATF4 expression pattern. As such, manipulations of enteral fat composition and treatment with hydrophilic bile acids may prove clinically useful in severe hepatic injury secondary to massive intestinal resection.

A well-established consequence of chronic ERS is dysregulation of the UPR with resultant preferential activation of proapoptotic over prosurvival pathways (7–9). This ERS-induced cell death is driven by CHOP, which is typically transcriptionally activated by ATF4 (9). After proximal SBR, the incitation of ER stress is likely multifactorial. It is known that intestinal permeability and bacterial translocation are increased following SBR in a TLR4-dependent manner (22, 23). The resultant proinflammatory milieu is further exacerbated by significant resection-induced dysbiosis (11, 24). This is consistent with the increased hepatic TNFα mRNA seen in the proximal SBR cohort. Another significant factor is oxidative stress, which is both a reported cause and effect of ERS. Reactive oxygen species are known by-products of protein folding pathways (25). However, impairment of the reduction-oxidation balance can disrupt such cellular functions causing accumulation of misfolded proteins and consequent ER stress (8). Onufer et. al. (26) demonstrated increased hepatic expression of oxidative stress markers after SBR in our murine SBR model, further supporting the notion that ERS and a maladaptive UPR are fundamental drivers of resection-associated liver injury.

Novel to this study, SBR-induced liver injury is associated with an inverse relationship between CHOP and its upstream effector ATF4, which is typically proportionate in both magnitude and direction. During ER stress, PERK phosphorylation of eIF2α represses global protein synthesis to reduce the protein-

folding load, with the notable exception of ATF4 translation that is selectively upregulated (27). It has previously been reported that a cell's fate is dependent on the extent and duration of ATF4 expression with subsequent induction of its proapoptotic target gene CHOP. However, several studies have demonstrated enhanced CHOP and UPR activity independent of ATF4 (27–29). Al-Baghdadi et al. (28) showed that global ATF4 KO mice still displayed a robust hepatic ER stress signature in response to treatment with asparaginase. Fusakio et al. (27) similarly found that ATF4 was not required for CHOP expression in livers subjected to ERS and that loss of ATF4 led to enhanced oxidative stress and increased free, hepatotoxic cholesterol in the liver. Finally, Zhao et. al. observed a decrease in hepatic ATF4 protein expression in response to both carbon tetrachloride (CCl4) and lipopolysaccharide/D-galactosamine (LPS/D-GalN)-induced liver injury. In that study, diminished ATF4 expression was exacerbated, whereas overexpression abrogated liver damage (29). These reports are aligned with our findings. Herein, mice with SBR-induced liver injury and fibrosis had absent hepatic ATF4 signal despite robust CHOP expression, whereas the hepato-protected mice demonstrated an inverse UPR activation pattern with increased ATF4 and severely diminished CHOP. Upregulation of ATF4 in this setting could signify appropriate curtailing of a maladaptive UPR. It could also represent the resumption of the myriad of other critical intracellular processes in which ATF4 is intimately involved, including glucose and lipid metabolism, nutrient stress sensing, amino acid metabolism, and redox homeostasis (30–33).

Manipulation of dietary fat mitigated hepatic damage and fibrosis after SBR and was associated with diminished CHOP expression in the liver. In the 2-wk diet experimental arm, HFD (35% kcal fat) was found to be injurious to the liver after SBR. It is important to note that diet alone did not induce the UPR and that the additional hit of the SBR-induced proinflammatory, prooxidative stress milieu was necessary. Transitioning the SBR mice to SC LFD (13% kcal fat) at 1 wk not only significantly abrogated the liver injury and fibrosis phenotype but also reversed the expression of CHOP/ATF4 compared with HFD-SBR counterparts, like what was seen in sham controls. This speaks to the critical importance of optimal enteral fat composition after massive intestinal resection, which is not yet well characterized. High-fat enteral feeding has numerous theoretical benefits including increased caloric density and enhanced intestinal mucosal adaptation response (34, 35). Breast milk, which is high in fat, remains the first choice of enteral feeds for SGS infants and children when available (35, 36). However, overfeeding with enteral HFD has also been associated with steatohepatitis (37). Type of fat plays an important role as well with long-chain and medium-chain fatty acids stimulating adaptation and augmenting absorption, respectively (38). Onufer et. al. (12) demonstrated that although fat load was likely a driver of steatosis, it was not sufficient to induce fibrosis in the absence of SBR. Taken together, this data underscores the importance of optimized enteral nutritional composition in the setting of SBR-associated liver injury.

Administration of TUDCA, an endogenous hydrophilic bile acid, was found to overcome the effects of diet plus resection at 10 wk. Not only was the fibrotic phenotype rescued, but intestinal adaptation was maximized and there was complete reversal of the hepatic UPR activation pattern. It is understood that massive intestinal resection results in significant alterations to the bile acid composition. In a piglet model of short bowel syndrome-associated liver disease (SBS-ALD), Pereira-Fantini et al. (39) reported marked changes, with pathophysiological implications, in the portal venous pool. Compared with shams, the SBS-ALD cohort was found to have a predominantly hydrophobic, liver-injurious primary bile acid pool with a fivefold increase in chenodeoxycholic acid (CDCA) (39). Here, TUDCA not only protects hepatocytes from the toxic hydrophobicity of other bile acid species but also has known therapeutic benefits in the setting of ER stress-induced liver disease (40). Paridaens et al. (41) found that TUDCA significantly mitigated end-stage liver injury in a murine model of secondary biliary fibrosis via reduction of hepatic CHOP-induced proapoptotic pathways. Another study showed suppression of hepatocarcinogen-driven ER stress by dampening UPR-activated apoptosis and inflammation in the liver (20). Finally, TUDCA has both potent antioxidant and anti-inflammatory properties (42), which further underscores the significance of these potential drivers in the current model of resection-associated liver injury. Treatment with other antioxidants such as allopurinol and superoxide dismutase after SBR could be invaluable future directions to help delineate the importance of these insults in the resultant hepatic phenotype.

Distal SBR, a selective removal of the terminal ileum and cecum, also mitigated liver injury and fibrosis with a similar UPR activation pattern as seen in TUDCA-treated mice. The critical importance of the location and functionality of the anatomical segmental resection in SGS is well documented. Previously, the ileum was presumed to have the greatest capacity for structural adaptation; "proximalizing" to compensate for the loss of upstream bowel (3, 43). A recent study by Han et al. (44) revealed that intestinal-derived high-density lipoprotein-3 (HDL3) functioned to insulate bacterial lipopolysaccharide (LPS) after SBR thus protecting the liver from subsequent inflammation and injury. Contrary to the results of the current study, ileal resection was associated with an exacerbated liver injury phenotype compared with proximal resection (44). One potential explanation for these disparate findings is that Han et al. (45) left the cecum in situ, anastomosing the proximal jejunum to a cuff of the terminal ileum, whereas in our current distal SBR model, the ileum and cecum were both resected en bloc. One function of the cecum is to slow intestinal transit. This could therefore encourage greater dysbiosis within the remnant jejunum, which has greater permeability at baseline (45). These findings emphasize the nuanced contributions of respective segments of the gastrointestinal tract. Finally, bile acid dysregulation and the accumulation of hepatotoxic bile acid species can itself induce ER stress and the UPR, as discussed above. Thompson et al. (46) demonstrated that perturbations in the cecal microbiome affected bile acid homeostasis. Recipients of cecal microbiome transplant from offspring exposed to maternal HFD were found to have increased bile acid pool size and altered hepatic bile acid profiles that led to a compensatory cytotoxic retention of bile acids in hepatocytes (46). It is plausible that fecal bile acid losses, combined with forfeiture of the absorptive capacity in the ileum and cecum and contributions from the cecal microbiome

could mitigate the additional bile acid burden on the liver after SBR. A more precise understanding of the contributions of the remnant small intestine and colon to liver injury after SBR is imperative.

Although increased CHOP expression in the liver is correlated with a greater degree of injury and fibrosis, global CHOP KO only partially prevented the hepatic phenotype after SBR. This suggests that CHOP contributes but is not essential for the induction of resection-associated liver injury. Interestingly, there were significant increases in ATF4 mRNA and protein in the liver conveying presumptive activation of the PERK arm of the UPR in the CHOP KO SBR cohort. This null effect of CHOP deficiency has been previously reported in the literature. Campos et al. (47) found that genetic depletion of CHOP did not abrogate carbon tetrachloride-induced liver damage by biochemical serum markers or volume of cell death. Similarly, Borkham–Kamphorst et al. (21) demonstrated that CHOP-null hepatocytes were not protected from late ERS-induced apoptosis after prolonged exposure to tunicamycin in vitro. These findings were attributed to the presence of compensatory mechanisms in the liver as well as the cross talk between the three arms of the UPR (21). It should be noted that the CHOP KO SBR cohort was the only experimental arm to demonstrate decreased apoptotic rate by cleaved caspase-3 protein expression, to a level comparable with sham WT controls. This finding emphasizes the complex relationship between CHOP and apoptosis and could be responsible for the limited hepatoprotection conferred by CHOP KO. Investigation of resection-associated liver injury phenotype in ATF4 KO mice and the differential activation of ERS-induced cell death would be important in future directions.

Finally, it is important to note the disparate ATF4 findings at the transcript and protein levels. Despite significant changes in hepatic protein expression with diminished signal in the liver-injured mice and increased signal in the hepato-protected experimental groups, there was no difference in relative mRNA gene expression. A likely contributor is nonsense-mediated mRNA decay (NMD), a highly selective degradation pathway that is involved in the tight regulation of the UPR (48–51). The NMD prevents premature or prolonged activation of the UPR through posttranscriptional degradation of target genes. Conversely, it is inhibited in response to severe ER stress to allow for full expression of the UPR and attempted return of the cell to baseline homeostatic conditions (48, 50). During chronic ER stress, when the UPR shifts to maladaptive and proapoptotic effectors, the NMD can itself become dysregulated and prevent translation of ATF4 resulting in a relative increase of secondary cellular transcripts (52).

Conclusions

The current study identifies a novel mechanism for proximal SBR-induced hepatic injury and fibrosis involving chronic ER stress and a maladaptive UPR in the liver. Resection-associated liver damage is associated with induction of the PERK arm of the UPR with increased expression of canonical executor protein CHOP and a reciprocal reduction in its upstream driver, ATF4. A low-fat diet, TUDCA administration, and distal SBR rescued the hepatic phenotype and demonstrated reversal of the UPR activation pattern. These findings underscore the significance of the gut/liver axis after SBR and elucidate the potential for clinically targetable interventions to prevent the severe liver injury associated with intestinal failure.

ACKNOWLEDGMENTS

Graphical abstract created with Biorender.com.

GRANTS

This study was supported by the National Institutes of Health (NIH) Grants T32DK077653 (to A. E. Steinberger) and T32DK007120 (to M. E. Tecos); by Children's Surgical Sciences Research Institute of the St. Louis Children's Hospital Foundation (to B. W. Warner); by NIH Grants P30DK52574 Digestive Diseases Research Core Center of the Washington University School of Medicine (to N. O. Davidson); and NIH Grants DK 119437 (to N. O. Davidson), HL 151328 (to N. O. Davidson), R01DK112378 (to N. O. Davidson and D. C. Rubin), and R01DK128169 (to B. W. Warner, N. O. Davidson, and D. C. Rubin).

DISCLOSURES

No conflicts of interest, financial or otherwise, are declared by the authors.

AUTHOR CONTRIBUTIONS

A.E.S., M.E.T., N.O.D., J.G., and B.W.W. conceived and designed research; A.E.S., M.E.T., H.M.P., and J.G. performed experiments; A.E.S., M.E.T., H.M.P., and J.G. analyzed data; A.E.S., M.E.T., N.O.D., J.G., and B.W.W. interpreted results of experiments; A.E.S., M.E.T., and J.G. prepared figures; A.E.S. drafted manuscript; A.E.S., M.E.T., D.C.R., N.O.D., J.G., and B.W.W. edited and revised manuscript; A.E.S., M.E.T., D.C.R., N.O.D., J.G., and B.W.W. approved final version of manuscript.

REFERENCES

1. **Goulet O**, **Ruemmele F.** Causes and management of intestinal failure in children. *Gastroenterology* 130: S16–S28, 2006. doi:10.1053/j.gastro.2005.12.002.
2. **Squires RH**, **Duggan C**, **Teitelbaum DH**, **Wales PW**, **Balint J**, **Venick R**, **Rhee S**, **Sudan D**, **Mercer D**, **Martinez JA**, **Carter BA**, **Soden J**, **Horslen S**, **Rudolph JA**, **Kocoshis S**, **Superina R**, **Lawlor S**, **Haller T**, **Kurs-Lasky M**, **Belle SH.** Natural history of pediatric intestinal failure: initial report from the Pediatric Intestinal Failure Consortium. *J Pediatr* 161: 723–728.e2, 2012. doi:10.1016/j.jpeds.2012.03.062.
3. **Shakhsheer BA**, **Warner BW.** Short bowel syndrome. *Curr Treat Options Pediatr* 5: 494–505, 2019. doi:10.1007/s40746-019-00179-y.
4. **Bishay M**, **Pichler J**, **Horn V**, **Macdonald S**, **Ellmer M**, **Eaton S**, **Hill S**, **Pierro A.** Intestinal failure-associated liver disease in surgical infants requiring long-term parenteral nutrition. *J Pediatr Surg* 47: 359–362, 2012. doi:10.1016/j.jpedsurg.2011.11.032.
5. **Pironi L**, **Sasdelli AS.** Intestinal failure-associated liver disease. *Clin Liver Dis* 23: 279–291, 2019. doi:10.1016/j.cld.2018.12.009.
6. **Courtney CM**, **Warner BW.** Pediatric intestinal failure-associated liver disease. *Curr Opin Pediatr* 29: 363–370, 2017. doi:10.1097/MOP.0000000000000484.
7. **Hetz C.** The unfolded protein response: controlling cell fate decisions under ER stress and beyond. *Nat Rev Mol Cell Biol* 13: 89–102, 2012. doi:10.1038/nrm3270.
8. **Chong WC**, **Shastri MD**, **Eri R.** Endoplasmic reticulum stress and oxidative stress: a vicious nexus implicated in bowel disease pathophysiology. *Int J Mol Sci* 18: 771, 2017. doi:10.3390/ijms18040771.
9. **Liu X**, **Green RM.** Endoplasmic reticulum stress and liver diseases. *Liver Res* 3: 55–64, 2019. doi:10.1016/j.livres.2019.01.002.
10. **Woodward JM**, **Massey D**, **Sharkey L.** The long and short of IT: intestinal failure-associated liver disease (IFALD) in adults-

recommendations for early diagnosis and intestinal transplantation. *Frontline Gastroenterol* 11: 34–39, 2020. doi:10.1136/flgastro-2018-101069.

11. **Barron L**, **Courtney C**, **Bao J**, **Onufer E**, **Panni RZ**, **Aladegbami B**, **Warner BW.** Intestinal resection-associated metabolic syndrome. *J Pediatr Surg* 53: 1142–1147, 2018. doi:10.1016/j.jpedsurg.2018.02.077.
12. **Onufer EJ**, **Han Y-H**, **Czepielewski RS**, **Courtney CM**, **Sutton S**, **Randolph GJ**, **Warner BW.** Effects of high-fat diet on liver injury after small bowel resection. *J Pediatr Surg* 55: 1099–1106, 2020. doi:10.1016/j.jpedsurg.2020.02.037.
13. **Rani S**, **Sreenivasaiah PK**, **Kim JO**, **Lee MY**, **Kang WS**, **Kim YS**, **Ahn Y**, **Park WJ**, **Cho C**, **Kim DH.** Tauroursodeoxycholic acid (TUDCA) attenuates pressure overload-induced cardiac remodeling by reducing endoplasmic reticulum stress. *PLoS One* 12: e0176071, 2017. doi:10.1371/journal.pone.0176071.
14. **Nair AB**, **Jacob S.** A simple practice guide for dose conversion between animals and human. *J Basic Clin Pharm* 7: 27–31, 2016. doi:10.4103/0976-0105.177703.
15. **Helmrath MA**, **VanderKolk WE**, **Can G**, **Erwin CR**, **Warner BW.** Intestinal adaptation following massive small bowel resection in the mouse. *J Am Coll Surg* 183: 441–449, 1996.
16. **Tecos M**, **Steinberger A**, **Guo J**, **Warner B.** Distal small bowel resection yields enhanced intestinal and colonic adaptation. *J Surg Res* 273: 100–109, 2021. doi:10.1016/j.jss.2021.11.015.
17. **Wakeman D**, **Guo J**, **Santos JA**, **Wandu WS**, **Schneider JE**, **McMellen ME**, **Leinicke JA**, **Erwin CR**, **Warner BW.** p38 MAPK regulates Bax activity and apoptosis in enterocytes at baseline and after intestinal resection. *Am J Physiol Gastrointest Liver Physiol* 302: G997–G1005, 2012. doi:10.1152/ajpgi.00485.2011.
18. **Barron L**, **Sun RC**, **Aladegbami B**, **Erwin CR**, **Warner BW**, **Guo J.** Intestinal epithelial-specific mTORC1 activation enhances intestinal adaptation after small bowel resection. *Cell Mol Gastroenterol Hepatol* 3: 231–244, 2016. doi:10.1016/j.jcmgh.2016.10.006.
19. **Hou Y**, **Yang H**, **Cui Z**, **Tai X**, **Chu Y**, **Guo X.** Tauroursodeoxycholic acid attenuates endoplasmic reticulum stress and protects the liver from chronic intermittent hypoxia induced injury. *Exp Ther Med* 14: 2461–2468, 2017. doi:10.3892/etm.2017.4804.
20. **Vandewynckel Y-P**, **Laukens D**, **Devisscher L**, **Paridaens A**, **Bogaerts E**, **Verhelst X**, **Van den Bussche A**, **Raevens S**, **Van Steenkiste C**, **Van Troys M**, **Ampe C**, **Descamps B**, **Vanhove C**, **Govaere O**, **Geerts A**, **Van Vlierberghe H.** Tauroursodeoxycholic acid dampens oncogenic apoptosis induced by endoplasmic reticulum stress during hepatocarcinogen exposure. *Oncotarget* 6: 28011–28025, 2015. doi:10.18632/oncotarget.4377.
21. **Borkham-Kamphorst E**, **Haas U**, **Van de Leur E**, **Trevanich A**, **Weiskirchen R.** Chronic carbon tetrachloride applications induced hepatocyte apoptosis in lipocalin 2 null mice through endoplasmic reticulum stress and unfolded protein response. *Int J Mol Sci* 21: 5230, 2020. doi:10.3390/ijms21155230.
22. **O'Brien DP**, **Nelson LA**, **Kemp CJ**, **Williams JL**, **Wang Q**, **Erwin CR**, **Hasselgren P-O**, **Warner BW.** Intestinal permeability and bacterial translocation are uncoupled after small bowel resection. *J Pediatr Surg* 37: 390–394, 2002. doi:10.1053/jpsu.2002.30807.
23. **Courtney CM**, **Onufer EJ**, **McDonald KG**, **Steinberger AE**, **Sescleifer AM**, **Seiler KM**, **Tecos ME**, **Newberry RD**, **Warner BW.** Small bowel resection increases paracellular gut barrier permeability via alterations of tight junction complexes mediated by intestinal TLR4. *J Surg Res* 258: 73–81, 2021. doi:10.1016/j.jss.2020.08.049.
24. **Engelstad HJ**, **Barron L**, **Moen J**, **Wylie TN**, **Wylie K**, **Rubin DC**, **Davidson N**, **Cade TW**, **Warner BB**, **Warner BW.** Remnant small bowel length in pediatric short bowel syndrome and the correlation with intestinal dysbiosis and linear growth. *J Am Coll Surg* 227: 439–449, 2018. doi:10.1016/j.jamcollsurg.2018.07.657.
25. **Plaisance V**, **Brajkovic S**, **Tenenbaum M**, **Favre D**, **Ezanno H**, **Bonnefond A**, **Bonner C**, **Gmyr V**, **Kerr-Conte J**, **Gauthier BR**, **Widmann C**, **Waeber G**, **Pattou F**, **Froguel P**, **Abderrahmani A.** Endoplasmic reticulum stress links oxidative stress to impaired pancreatic beta-cell function caused by human oxidized LDL. *PLoS One* 11: e0163046, 2016. doi:10.1371/journal.pone.0163046.
26. **Onufer EJ**, **Han Y-H**, **Courtney C**, **Steinberger A**, **Tecos M**, **Sutton S**, **Sescleifer A**, **Ou J**, **Sanguinetti Czepielewski R**, **Randolph GJ**, **Warner BW.** Liver injury after small bowel resection is prevented in obesity-resistant 129S1/SvImJ mice. *Am J Physiol Gastrointest Liver Physiol* 320: G907–G918, 2021. doi:10.1152/ajpgi.00284.2020.
27. **Fusakio ME**, **Willy JA**, **Wang Y**, **Mirek ET**, **Al Baghdadi RJT**, **Adams CM**, **Anthony TG**, **Wek RC.** Transcription factor ATF4 directs basal and stress-induced gene expression in the unfolded protein response and cholesterol metabolism in the liver. *Mol Biol Cell* 27: 1536–1551, 2016. doi:10.1091/mbc.E16-01-0039.
28. **Al-Baghdadi RJT**, **Nikonorova IA**, **Mirek ET**, **Wang Y**, **Park J**, **Belden WJ**, **Wek RC**, **Anthony TG.** Role of activating transcription factor 4 in the hepatic response to amino acid depletion by asparaginase. *Sci Rep* 7: 1272, 2017. doi:10.1038/s41598-017-01041-7.
29. **Zhao X**, **Zhou H**, **Cheng Y**, **Yu W**, **Luo G**, **Duan C**, **Yao F**, **Xiao B**, **Feng C**, **Xia X**, **Wei M**, **Wang Y**, **Li J**, **Dai R.** Reduction in activating transcription factor 4 promotes carbon tetrachloride and lipopolysaccharide/D-galactosamine-mediated liver injury in mice. *Mol Med Rep* 18: 1718–1725, 2018. doi:10.3892/mmr.2018.9080.
30. **Seo H-Y**, **Kim M-K**, **Min A-K**, **Kim H-S**, **Ryu S-Y**, **Kim N-K**, **Lee KM**, **Kim H-J**, **Choi H-S**, **Lee K-U**, **Park K-G**, **Lee I-K.** Endoplasmic reticulum stress-induced activation of activating transcription factor 6 decreases cAMP-stimulated hepatic gluconeogenesis via inhibition of CREB. *Endocrinology* 151: 561–568, 2010. doi:10.1210/en.2009-0641.
31. **Wang C**, **Huang Z**, **Du Y**, **Cheng Y**, **Chen S**, **Guo F.** ATF4 regulates lipid metabolism and thermogenesis. *Cell Res* 20: 174–184, 2010. doi:10.1038/cr.2010.4.
32. **Lange PS**, **Chavez JC**, **Pinto JT**, **Coppola G**, **Sun C-W**, **Townes TM**, **Geschwind DH**, **Ratan RR.** ATF4 is an oxidative stress-inducible, prodeath transcription factor in neurons in vitro and in vivo. *J Exp Med* 205: 1227–1242, 2008. doi:10.1084/jem.20071460.
33. **Kilberg MS**, **Shan J**, **Su N.** ATF4-dependent transcription mediates signaling of amino acid limitation. *Trends Endocrinol Metab* 20: 436–443, 2009. doi:10.1016/j.tem.2009.05.008.
34. **Ou J**, **Courtney CM**, **Steinberger AE**, **Tecos ME**, **Warner BW.** Nutrition in necrotizing enterocolitis and following intestinal resection. *Nutrients* 12: 520, 2020. doi:10.3390/nu12020520.
35. **Olieman JF**, **Penning C**, **Ijsselstijn H**, **Escher JC**, **Joosten KF**, **Hulst JM**, **Tibboel D.** Enteral nutrition in children with short-bowel syndrome: current evidence and recommendations for the clinician. *J Am Diet Assoc* 110: 420–426, 2010. doi:10.1016/j.jada.2009.12.001.
36. **Morgan J**, **Young L**, **McGuire W.** Slow advancement of enteral feed volumes to prevent necrotising enterocolitis in very low birth weight infants. *Cochrane Database Syst Rev* 10: CD001241, 2015. doi:10.1002/14651858.CD001241.
37. **Ito M**, **Suzuki J**, **Tsujioka S**, **Sasaki M**, **Gomori A**, **Shirakura T**, **Hirose H**, **Ito M**, **Ishihara A**, **Iwaasa H**, **Kanatani A.** Longitudinal analysis of murine steatohepatitis model induced by chronic exposure to high-fat diet. *Hepatol Res* 37: 50–57, 2007. doi:10.1111/j.1872-034X.2007.00008.x.
38. **Choi PM**, **Sun RC**, **Guo J**, **Erwin CR**, **Warner BW.** High-fat diet enhances villus growth during the adaptation response to massive proximal small bowel resection. *J Gastrointest Surg* 18: 286–294, 2014. doi:10.1007/s11605-013-2338-7.
39. **Pereira-Fantini PM**, **Lapthorne S**, **Joyce SA**, **Dellios NL**, **Wilson G**, **Fouhy F**, **Thomas SL**, **Scurr M**, **Hill C**, **Gahan CGM**, **Cotter PD**, **Fuller PJ**, **Hardikar W**, **Bines JE.** Altered FXR signalling is associated with bile acid dysmetabolism in short bowel syndrome-associated liver disease. *J Hepatol* 61: 1115–1125, 2014. doi:10.1016/j.jhep.2014.06.025.
40. **Lu Q**, **Jiang Z**, **Wang Q**, **Hu H**, **Zhao G.** The effect of Tauroursodeoxycholic acid (TUDCA) and gut microbiota on murine gallbladder stone formation. *Ann Hepatol* 23: 100289, 2021. doi:10.1016/j.aohep.2020.100289.
41. **Paridaens A**, **Raevens S**, **Devisscher L**, **Bogaerts E**, **Verhelst X**, **Hoorens A**, **Van Vlierberghe H**, **van Grunsven LA**, **Geerts A**, **Colle I.** Modulation of the unfolded protein response by tauroursodeoxycholic acid counteracts apoptotic cell death and fibrosis in a mouse model for secondary biliary liver fibrosis. *Int J Mol Sci* 18: 214, 2017. doi:10.3390/ijms18010214.
42. **Portincasa P**, **Grattagliano I**, **Testini M**, **Caruso M**, **Wang D**, **Moschetta A**, **Calamita G**, **Vacca M**, **Valentini A**, **Renna G.** Parallel intestinal and liver injury during early cholestasis in the rat: modulation by bile salts and antioxidants. *Free Radic Biol Med* 42: 1381–1391, 2007. doi:10.1016/j.freeradbiomed.2007.01.039.
43. **Longshore SW**, **Wakeman D**, **McMellen M**, **Warner BW.** Bowel resection induced intestinal adaptation: progress from bench to bedside. *Minerva Pediatr* 61: 239–251, 2009.

44. **Han Y-H**, **Onufer EJ**, **Huang L-H**, **Sprung RW**, **Davidson WS**, **Czepielewski RS**, **Wohltmann M**, **Sorci-Thomas MG**, **Warner BW**, **Randolph GJ.** Enterically derived high-density lipoprotein restrains liver injury through the portal vein. *Science* 373: eabe6729, 2021. doi:10.1126/science.abe6729.
45. **Collins FL**, **Rios-Arce ND**, **Atkinson S**, **Bierhalter H**, **Schoenherr D**, **Bazil JN**, **McCabe LR**, **Parameswaran N.** Temporal and regional intestinal changes in permeability, tight junction, and cytokine gene expression following ovariectomy-induced estrogen deficiency. *Physiol Rep* 5: e13263, 2017. doi:10.14814/phy2.13263.
46. **Thompson MD**, **Kang J**, **Faerber A**, **Hinrichs H**, **Özler O**, **Cowen J**, **Xie Y**, **Tarr PI**, **Davidson NO.** Maternal obesogenic diet regulates offspring bile acid homeostasis and hepatic lipid metabolism via the gut microbiome in mice. *Am J Physiol Gastrointest Liver Physiol* 322: G295–G309, 2022. doi:10.1152/ajpgi.00247.2021.
47. **Campos G**, **Schmidt-Heck W**, **Ghallab A**, **Rochlitz K**, **Pütter L**, **Medinas DB**, **Hetz C**, **Widera A**, **Cadenas C**, **Begher-Tibbe B**, **Reif R**, **Günther G**, **Sachinidis A**, **Hengstler JG**, **Godoy P.** The transcription factor CHOP, a central component of the transcriptional regulatory network induced upon CCl4 intoxication in mouse liver, is not a critical mediator of hepatotoxicity. *Arch Toxicol* 88: 1267–1280, 2014. doi:10.1007/s00204-014-1240-8.
48. **Karam R**, **Lou C-H**, **Kroeger H**, **Huang L**, **Lin JH**, **Wilkinson MF.** The unfolded protein response is shaped by the NMD pathway. *EMBO Rep* 16: 599–609, 2015. doi:10.15252/embr.201439696.
49. **Carreras-Sureda A**, **Hetz C.** RNA metabolism: putting the brake on the UPR. *EMBO Rep* 16: 545–546, 2015. doi:10.15252/embr.201540227.
50. **Goetz AE**, **Wilkinson M.** Stress and the nonsense-mediated RNA decay pathway. *Cell Mol Life Sci* 74: 3509–3531, 2017 [Erratum in *Cell Mol Life Sci* 74: 4047, 2017]. doi:10.1007/s00018-017-2537-6.
51. **Usuki F**, **Yamashita A**, **Fujimura M.** Environmental stresses suppress nonsense-mediated mRNA decay (NMD) and affect cells by stabilizing NMD-targeted gene expression. *Sci Rep* 9: 1279, 2019. doi:10.1038/s41598-018-38015-2.
52. **Mannaerts I**, **Thoen LFR**, **Eysackers N**, **Cubero FJ**, **Batista Leite S**, **Coldham I**, **Colle I**, **Trautwein C**, **van Grunsven LA.** Unfolded protein response is an early, non-critical event during hepatic stellate cell activation. *Cell Death Dis* 10: 98, 2019. doi:10.1038/s41419-019-1327-5.